Crystallization mechanism of Cu-based supercooled liquid under ambient and high pressure

Z. X. Wang, D. Q. Zhao, M. X. Pan, P. Wen, and W. H. Wang*

Institute of Physics, Chinese Academy of Sciences, Beijing 100080, People's Republic of China

T. Okada and W. Utsumi

Japan Atomic Energy Research Institute, Spring-8, Hyogo 679-5198, Japan

Crystallization of a $Cu_{60}Zr_{20}Hf_{10}Ti_{10}$ bulk metallic glass in the entire supercooled liquid region (SLR) is studied using an *in situ* x-ray diffraction with synchrotron radiation under high pressure and a differential scanning calorimeter at ambient pressure. The temperature-time-transition diagrams under ambient and high pressure are determined and compared, and the phase evolution of the crystallization with time is *in situ* exhibited under high pressure. We find that the crystallization in the temperature regime near glass transition temperature and near melting temperature in SLR cannot be described by a single crystallization mechanism in the entire SLR under high pressure. The effects of pressure on the crystallization of the BMG are explored.

Crystallization studies of bulk metallic glasses (BMGs) are of importance in understanding mechanisms of phase transformations far form equilibrium, evaluating the glass formation ability of the melts, and producing controlled ultra-refined microstructure.[1–3] Recently, Cu-based BMGs were developed, and they were found to have a high thermal stability against crystallization and excellent mechanical properties.[4,5] The $Cu_{60}Zr_{20}Hf_{10}Ti_{10}$ alloy is a typical Cu-based BMG which has a large supercooled region (SLR) and high thermal stability which lead to a large experimentally accessible time and temperature window to investigate the transformation from amorphous to crystal under isothermal condition in SLR. The characterization of the time scale for isothermal condition is given by the temperature-time-transition (TTT) diagram which can determine the time scale to reach the onset of crystallization and confirm the theoretically predicted nose shape and provide important information about glass forming ability, nucleation mechanism of a system.[6,7] The TTT diagram for a metallic system is usually determined by an electrostatic levitator[8] or by inductively heating the samples in a graphite crucible.[9,10] With the development of a high pressure technique, pressure to the advancement of science and technology has become more important, similar to that of a temperature variable or a composition variable.[11] However, there is little information about the pressure-temperature-time-transition (PTTT) diagram for metallic alloys, which could provide a deeper insight into the crystallization and glass forming mechanism of a glass forming liquid. On the other hand, the time dependence of the entire crystallization process, which is given by the time to reach the onset of crystallization and the time for the actual crystallization process to complete, has not been studied over the temperature and pressure ranges from the equilibrium liquid down to the glass transition temperature for glass forming alloys. In this letter, by using *in situ* high pressure and high temperature energy-dispersive x-ray diffraction (XRD) with synchrotron radiation, the PTTT diagrams of the $Cu_{60}Zr_{20}Hf_{10}Ti_{10}$ alloy was determined and compared with that at ambient pressure. The phase evolution of the crystallization process with time is *in situ* exhibited in

the entire SLR under isothermal conditions under high pressure. The crystallization kinetics and mechanism in the SLR and the effects of pressure on the crystallization of the Cu-based BMG are explored.

The $Cu_{60}Zr_{20}Hf_{10}Ti_{10}$ BMG was prepared by die casting the melt in a water-cooling Cu mold.[12–14] Crystallization experiments under ambient pressure were carried out under a purified argon atmosphere in a Perkin-Elmer DSC7. The calorimeter was calibrated for temperature and energy with high purity indium and zinc. The crystallization experiments under high temperature and high pressure were studied by an *in situ* XRD at SPring8, the third-generation synchrotron facility in Japan. High-pressure and high-temperature conditions were generated using a cubic-type multi-anvil press (SMAP 180) install on BL14B1 at SPring8.[15] The sample assembly was similar to that used in Ref. 16. A NiCr-NiAl thermocouple was brought into the pressurized zone and near the sample. NaCl powder was used as pressure transmitting medium. The pressure was calibrated from the lattice constant of NaCl. The accuracy was better than ± 0.2 GPa. An energy dispersive method was utilized using a white x ray with an energy of 20–150 keV. The diffracted x ray was detected by a solid state Ge detector; the diffraction angle 2θ was fixed to $3°$.

The glass transition temperature T_g, onset crystallization temperature T_x, and melting temperature T_m, of the Cu-based BMG at ambient condition are 734, 782, and 1189 K, respectively.[14] Figure 1 shows the isothermal differential scanning calorimeter (DSC) traces of the BMG at different temperatures. For an isothermal anneal at 748 K, the time to reach the onset crystallization, t_{onset}, takes 72 s, and the end crystallization time, t_{end} is 510 s. t_{onset} and t_{end} for different isothermal anneals are plotted as functions of the temperature and shown in the inset of Fig. 1. In the TTT diagram, a part of the typical "nose" shape for the onset time can be seen. Both t_{onset} and the entire crystallization time, $t_{end} - t_{onset}$, increase with decreasing temperature, indicating that the crystallization process needs longer time at lower temperature in the SRL. Assuming that the heat flow measured upon crystallization in the DSC is proportional to the
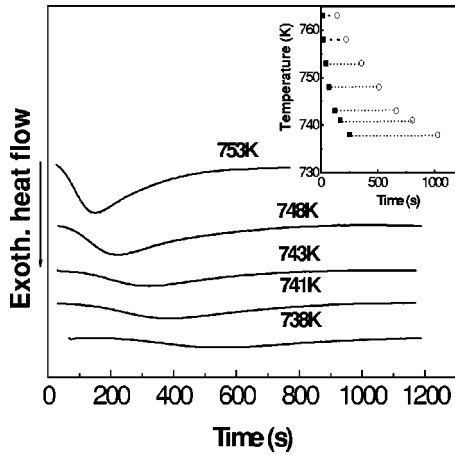
FIG. 1. The DSC curves for the $Cu_{60}Zr_{20}Hf_{10}Ti_{10}$ BMG at different isothermal temperatures. The inset shows the TTT diagram for the BMG. (■) is the onset time of the crystallization, and (○) the end time of crystallization.

crystallization rate, and the crystallization enthalpy is proportional to the crystallized volume fraction. The crystallized volume fraction, x with the isothermal time at different temperatures can be obtained and shown in Fig. 2. The shape of the x-t curves is typical "S" type. We tried to use the Johnson-Mehl-Avrami-Kolmogorov (JMAK) equation,[17–19] $x = 1 - \exp(-k(t-\tau))^n$, which based on the steady state nucleation model, to simulate the crystallization. In the equation k is the rate constant, $\tau = t_{onset}$, the incubation time, and n is a constant depending on the reaction mechanism. The inset is the linear fits between $\ln(-\ln(1-x))$ and $\ln(t-\tau)$ at different temperatures. The fit values of k and n are listed in Table I. The satisfactory fit shown in Fig. 2 indicates that the crystallization at ambient condition meets the steady state nucleation model, and the set of virtually parallel fit lines shown in the inset indicates that the crystallization reaction is isokinetic over this temperature range in the BMG.

Figures 3(a) and 3(b) exhibit the *in situ* recorded XRD patterns of the BMG at temperature regimes near T_g and T_m
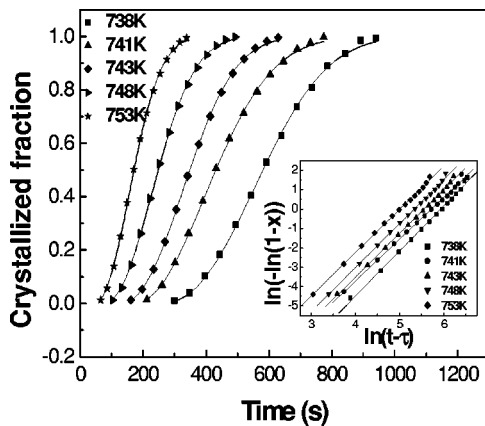
TABLE I. The values of k and n of the Cu-based BMG at different temperatures and pressures. The values of k and n are obtained by a linear fit between $\ln(-\ln(1-x))$ and $\ln(t-\tau)$.

Pressure	Temperature (K)	n	$k*10^{-3}$ (s^{-1})
ambient	738	2.34 ± 0.04	2.59 ± 0.01
	741	2.08 ± 0.02	3.21 ± 0.01
	743	2.22 ± 0.02	3.80 ± 0.01
	748	2.17 ± 0.02	4.79 ± 0.01
	753	2.13 ± 0.02	6.64 ± 0.02
4.5 GPa	863	1.03 ± 0.14	2.6 ± 0.7
	843	0.81 ± 0.05	4.5 ± 1.4

in the SLR under 4.5 GPa respectively. When the melt alloy was kept at 1193 K (near T_m, cooled from 1373 K with 7 K/s), it almost fully crystallizes in 30 s, as shown in Fig. 3(a). The rapid crystallization makes difficult to study the isothermal crystallization near T_m in the SLR. At temperature regime near T_g in SLR, such as at 843 K, however, the supercooled liquid state is much stable, and it can be kept until iso-annealed for 500 s [see Fig. 3(b)]. The sluggish crystallization kinetics make it possible for us to study the isothermal crystallization near T_g. When there are some very small crystalline peaks appear meaning of the beginning of the crystallization, we defined the time when the crystalline phase can be detected by XRD as t_{onset}. With increasing time, the crystalline peaks become sharper and stronger, meaning that the crystalline volume fraction increases with increasing annealing time. The BMG mainly crystallizes into $Cu_{10}Zr_7$- type and ω-(Cu,Zr)-type crystalline phases which are much different from the crystallized phases from the melt in Fig. 3(a). Our experimental results also show that the product crystallized phases are identical at ambient pressure and high pressure, which will be published elsewhere. Unlike the crystallization in other BMGs, no metastable crystalline phases precipitate during the isothermal crystallization.[20,21] Up to $t=2400$ s, the sample is only about

FIG. 2. The crystallized volume fraction at different isothermal temperatures and times of the $Cu_{60}Zr_{20}Hf_{10}Ti_{10}$ BMG. The inset is the plot of the JMAK relationship at different isothermal temperatures of the BMG.
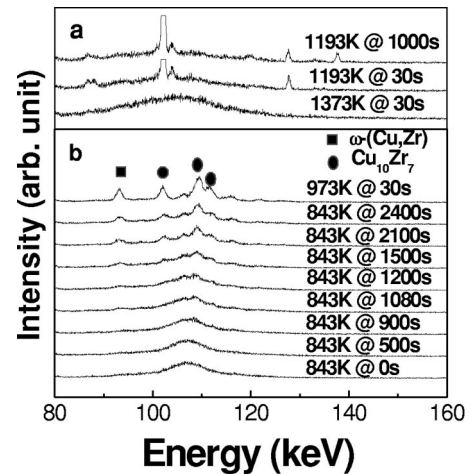
FIG. 3. The XRD patterns of the BMG at various isothermal temperatures and times under 4.5 GPa. (a) at temperature regime near T_m in SRL, and (b) at temperature regime near T_g. in SRL.
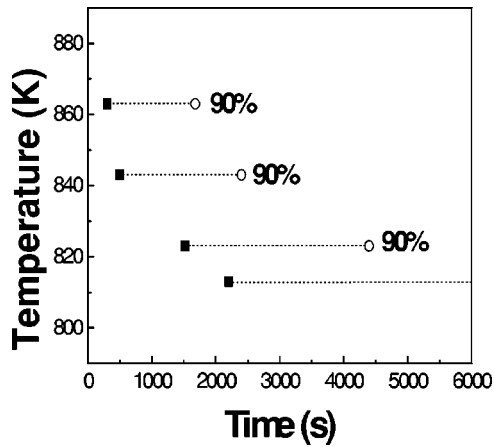
FIG. 4. PTTT diagram of the $Cu_{60}Zr_{20}Hf_{10}Ti_{10}$ BMG under 4.5 GPa in a temperature regime near T_g. in SRL. (■) is the onset time of the crystallization, and (○) the time of crystallized volume fraction 90%.

FIG. 5. The crystallized volume fraction at different isothermal times of the $Cu_{60}Zr_{20}Hf_{10}Ti_{10}$ BMG at 843 K under 4.5 GPa. The inset shows the plots of the JMAK relationship.

90% crystallized. No contaminant material can be detected by the *in situ* XRD during the isothermal crystallization process in the temperature regime near T_g in SLR as shown in Fig. 3(b). Isothermal experiments at 4.5 GPa were carried out at different temperatures near T_g in the SLR, and the results are summarized in the PTTT diagram and shown in Fig. 4. It can be clearly seen that the entire crystallization time increases with decreasing isothermal temperature. Above results show that the onset crystallization time, the entire crystallization time and the crystalline products for isothermal annealed near T_g or near T_m in the SLR under high pressure (HP) are obviously different as shown in Figs. 3(a) and 3(b). The phenomena imply that the nucleation and growth mechanisms are different at the two temperature regimes in SLR under HP. Similar results have been found in PdNiCuP and Vit1 BMGs at ambient pressure.[8,22,23] In those BMGs, once crystallization takes place for the isothermal annealing near T_m in the SLR, it will finish in a very short time. While when they were isothermal annealed near T_g, the entire crystallization time, $t_{end} - t_{onset}$, becomes much longer and increases with decreasing temperature. The crystallization is considered as a nucleation-controlled process near T_m, and a growth-controlled process near T_g in these BMGs.[8,22,23] Our results show the similar characters of a growth-controlled process in the temperature regime near T_g both at ambient pressure and 4.5 GPa. At temperature regime neat T_m, the crystallization of the Cu-based BMG under high pressure is very sensitive to heterogeneous nucleation sites, and could be regarded as a nucleation controlled process based on similarity with others results. Because the specimen was covered with a pressure transmitting medium which provides a high density of heterogeneous nucleation sites, the crystallization then occurs with a very short incubation time and an entire crystallization time. While near T_g in the SLR, the crystallization is a growth-controlled process, and the growth of crystals solely determines the time scale of the crystallization. The quenched-in preexisting nuclei and the high density of heterogeneous nucleation sites from the pressure transmitting medium have no significant effect on
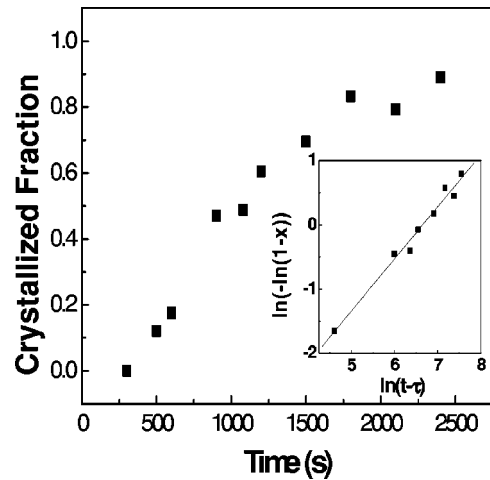
the crystallization. The above results indicate that the entire crystallization in the SLR depends on the temperature scale, and the single concept of a steady-state nucleation mechanism cannot provide an adequate description of the nucleation process in the whole SLR.

To determine the crystallized volume fraction, x during the *in situ* isothermal crystallization process near T_g in the SLR under high pressure, we calculated x by assuming that each XRD pattern is a linear combination of an amorphous part I_a (I_a is the integrated intensities of the XRD pattern for the full amorphous sample at $t=0$), recorded at $t=0$, and a crystallized part I_c (I_a is the integrated intensities of the fully crystallized amorphous sample calculated by fitting the diffraction peaks with a Gaussian function), recorded at t_{end}. Therefore, the whole intensity at time t is $I(t) = (1-x)I_a + xI_c$. x then can be determined from the expression. At an isothermal annealing temperature near T_g which is much low than T_m. the estimation is not unreasonable because the intensity of the crystalline phase is roughly proportional to the volume of the phase and the effect of the contaminant material can be neglected. However, in the isothermal annealing temperature near T_m, the method cannot be used to estimate x because of the possible effect of the contaminant material on the accuracy of the intensity determination. As an example, the calculated x curve for isothermal annealing at 843 K at 4.5 GPa is shown in Fig. 5. The inset shows the linear relationship between $\ln[-\ln(1-x)]$ and $\ln(t-\tau)$. The satisfactory fits indicate that the crystallization under high pressure also meets the steady state nucleation model in the Cu-based BMG. The activation energy E_a can be estimated from the temperature dependent incubation time τ, roughly, we think $\tau = \tau_{onset} = \tau_0 \exp(E_a/k_B T)$, where τ_0 is a constant. The effective activation energy can be considered to be related mainly to the nucleation process, because during the initial crystallization stage, the incubation time period, nucleation is the dominant process. The obtained values of E_a deduced from $\ln t_{onset}$ vs $1/T$ are 5.77 ± 0.26 eV under ambient pressure and 2.52 ± 0.25 eV under 4.5 GPa, respectively. A large difference exists between the values of E_a under ambient and

high pressures. The nucleation activation energy is much decreased under high pressure, which means a much lower energy barrier for the nucleation. That is, high pressure promoted nucleation in the BMG under high pressure. High pressure promotes nucleation in the BMG by promoting a shot-range atomic rearrangement by reducing the free volume due to compression and the restructuring of the atomic configuration.[12]

According to classical theory, for $n > 4$, the nucleation frequency increases with the crystallization time, while, $3 \leq n \leq 4$, the nucleation frequency decreases.[24] In Cu-based BMG, the average value of n is about 2.1 at the isothermal annealing temperature regime near T_g under ambient pressure (see Table I). The experimentally determined values of n fall outside those expected by classical theory. These suggest that the nucleation is not the dominant factor in crystallization near T_g, and the crystallization is a growth-controlled process. The representative fitting values of n under high pressure annealing are also listed in Table I. The value of n decreases significantly under high pressure, e.g., $n = 1.03$ at 863 K and 4.5 GPa. The small value of n also implies a small nucleation activation energy under high pressure.[25] On the other hand, at a temperature near T_g, a high number density of the nuclei usually preexists in the alloy,[26] the preexisting high number density of the nuclei may result from high heterogeneous nucleation rates, quenched-in nuclei, or phase separation in the supercooled liquid prior to crystallization.[26] The observed phenomenon is that the entire crystallization time during isothermal annealing under high pressure becomes much longer compared to that at ambient condition, although the isothermal temperature increases much under high pressure. These further confirm the growth-controlled crystallization under high pressure near T_g. The effect of pressure on the growth-controlled crystallization near T_g is due to the suppression of the long-range diffusion process in the supercooled liquid state.[12] Comparing the TTT (in Fig. 1) and PTTT diagrams (in Fig. 4), one can see that applied pressure makes the TTT diagram shift to the high temperature region, and cause the entire crystallization time, $t_{end} - t_{onset}$ to be much extended.

In conclusion, the PTTT diagram of the $Cu_{60}Zr_{20}Hf_{10}Ti_{10}$ BMG is obtained and compared with its TTT diagram. The crystallization process of the BMG is found to be controlled by different mechanisms on different temperature scales in the supercooled liquid region. In the temperature region near T_g the crystallization is the growth-controlled process both at ambient and high pressures, while in the temperature regime near T_m it has the characteristic of a nucleation-controlled process. The applied pressure promotes the nucleation in the initial incubation time crystallization stage, and suppresses the growth process through the inhibition of the long-range diffusion process in crystallization.

---

*Contact author. Email address: whw@aphy.iphy.ac.cn

[1] A. L. Greer, Mater. Sci. Eng., A **179/180**, 41 (1996).

[2] H. S. Chen, J. Non-Cryst. Solids **27**, 257 (1978).

[3] M. C. Weinberg, Thermochim. Acta **280/281**, 63 (1996).

[4] W. L. Johnson, MRS Bull. **24**, 42 (1999).

[5] A. Inoue, W. Zhang, and K. Kurosaka, Mater. Trans., JIM **42**, 1805 (2001).

[6] D. Turnbull, J. Appl. Phys. **21**, 1022 (1950).

[7] D. R. Uhlmann, J. Non-Cryst. Solids **7**, 337 (1972).

[8] Y. J. Kim, R. Busch, and W. L. Johnson, Appl. Phys. Lett. **68**, 1057 (1996).

[9] J. Lüffler, J. Schroers, and W. L. Johnson, Appl. Phys. Lett. **77**, 681 (2000).

[10] J. Schroers, W. L. Johnson, and R. Busch, Appl. Phys. Lett. **77**, 1158 (2000).

[11] R. J. Hemley, L. C. Chen, and H. K. Mao, Nature (London) **338**, 638 (1989).

[12] W. H. Wang, D. W. He, and Y. S. Yao, Appl. Phys. Lett. **75**, 2770 (1999).

[13] W. H. Wang, Q. Wei, and S. Fridrich, Phys. Rev. B **57**, 8211 (1998).

[14] Z. X. Wang, D. Q. Zhao, M. X. Pan, and W. H. Wang, J. Phys.: Condens. Matter **15**, 5923 (2003).

[15] W. Utsumi and O. Shimomura, Rev. High Pressure Sci. Techno. **7**, 1484 (1998).

[16] V. Turkevich, T. Okada, and W. Utsumi, Diamond Relat. Mater. **11**, 1769 (2002).

[17] W. A. Johnson and R. F. Mehl, Trans. Am. Inst. Min. Met. Eng. **135**, 416 (1939).

[18] M. Avrami, J. Chem. Phys. **8**, 212 (1940).

[19] A. N. Kolmogorov, Izv. Acad. Nauk SSSR Ser. Math. **3**, 355 (1937).

[20] W. H. Wang, E. Wu, S. J. Kennedy, and A. J. Studer, Phys. Rev. B **66**, 104205 (2002).

[21] J. Eckert and L. Schultz, Mater. Trans., JIM **39**, 623 (1998).

[22] J. Schroers, Y. Wu, R. Busch, and W. L. Johnson, Acta Mater. **49**, 2773 (2001).

[23] J. Schroers, A. Masuhr, and W. L. Johnson, Phys. Rev. B **60**, 11 855 (1999).

[24] D. Turnbull, Phys. Solid State **3**, 225 (1956).

[25] J. W. Christian, *The Theory of Transformation in Metals and Alloys*, 2nd ed. (Pergamon Press, Oxford, 1975).

[26] T. Waniuk, J. Schroers, and W. L. Johnson, Phys. Rev. B **67**, 184203 (2003).